

## Review

Giovanna De Simone, Paolo Ascenzi\*, Alessandra di Masi and Fabio Polticelli

# Nitrophorins and nitrobindins: structure and function

DOI 10.1515/bmc-2017-0013

Received March 21, 2017; accepted May 3, 2017

**Abstract:** Classical all  $\alpha$ -helical globins are present in all living organisms and are ordered in three lineages: (i) flavohemoglobins and single domain globins, (ii) protoglobins and globin coupled sensors and (iii) truncated hemoglobins, displaying the 3/3 or the 2/2 all  $\alpha$ -helical fold. However, over the last two decades, all  $\beta$ -barrel and mixed  $\alpha$ -helical- $\beta$ -barrel heme-proteins displaying heme-based functional properties (e.g. ligand binding, transport and sensing) closely similar to those of all  $\alpha$ -helical globins have been reported. Monomeric nitrophorins (NPs) and  $\alpha_1$ -microglobulin ( $\alpha_1$ -m), belonging to the lipocalin superfamily and nitrobindins (Nbs) represent prototypical heme-proteins displaying the all  $\beta$ -barrel and mixed  $\alpha$ -helical- $\beta$ -barrel folds. NPs are confined to the Reduviidae and Cimicidae families of Heteroptera, whereas  $\alpha_1$ -m and Nbs constitute heme-protein families spanning bacteria to *Homo sapiens*. The structural organization and the reactivity of the stable ferric solvent-exposed heme-Fe atom suggest that NPs and Nbs are devoted to NO transport, storage and sensing, whereas *Hs*- $\alpha_1$ -m participates in heme metabolism. Here, the structural and functional properties of NPs and Nbs are reviewed in parallel with those of sperm whale myoglobin, which is generally taken as the prototype of monomeric globins.

**Keywords:** function; nitrobindin; nitrophorin; structure.

**\*Corresponding author: Paolo Ascenzi**, Department of Science, Roma Tre University, Viale Guglielmo Marconi 446, I-00146 Rome, Italy; and Interdepartmental Laboratory for Electron Microscopy, Roma Tre University, Via della Vasca Navale 79, I-00146 Rome, Italy, e-mail: ascenzi@uniroma3.it

**Giovanna De Simone and Alessandra di Masi:** Department of Science, Roma Tre University, Viale Guglielmo Marconi 446, I-00146 Rome, Italy; and Interdepartmental Laboratory for Electron Microscopy, Roma Tre University, Via della Vasca Navale 79, I-00146 Rome, Italy

**Fabio Polticelli:** Department of Science, Roma Tre University, Viale Guglielmo Marconi 446, I-00146 Rome, Italy; and National Institute of Nuclear Physics, Roma Tre Section, Roma Tre University, Via della Vasca Navale 84, I-00146 Rome, Italy. <http://orcid.org/0000-0002-7657-2019>

## Introduction

All  $\alpha$ -helical globins are present in all living organisms and are ordered in three lineages: (i) flavohemoglobins and single domain globins, (ii) protoglobins and globin coupled sensors and (iii) truncated hemoglobins. They perform a wide range of essential biological functions including ligand transport, storage and sensing, as well as heme-Fe-based catalysis (1–12).

Most of the all  $\alpha$ -helical globins [e.g. hemoglobin (Hb) and myoglobin (Mb)] display the classical 3/3 globin fold, made up of seven or eight  $\alpha$ -helical segments forming a sandwich around the heme. In particular, A-, B- and E- $\alpha$ -helices form one face of the sandwich, the other side being built by F-, G- and H- $\alpha$ -helices; C- and D- $\alpha$ -helices are very short, if present (2, 12–15). In the year 2000, a subset of the classical 3/3  $\alpha$ -helical sandwich was discovered and called 2/2 fold; this is essentially composed by B-, E-, G- and H- $\alpha$ -helices, which are arranged around the heme in a sort of bundle composed of anti-parallel pairs B/E and G/H connected by an extended polypeptide loop (16, 17). The heme is deeply buried in a crevice of the globin and is engaged in a number of hydrophobic contacts with the amino acid side chains paving the pocket which prevents the metal center oxidation (2, 10, 18, 19). The heme-Fe fifth coordination site is bound to the side chain of the so-called ‘proximal’ HisF8. The other axial position faces the so-called ‘distal’ E7 residue, which was demonstrated to contribute substantially to the stability of the heme-bound ligand and to the reversibility of the reaction. Of note, the occurrence of a His residue at the E7 position may lead to hexa-coordination of the heme Fe-atom impairing ligand binding (Figure 1) (2, 7, 12, 21–24).

Over the last two decades, monomeric all- $\beta$ -barrel and mixed- $\alpha$ -helical- $\beta$ -barrel heme-proteins have been reported to display heme-based functional properties (e.g. ligand transport, storage and sensing) similar to those of all  $\alpha$ -helical globins. They include *Rhodnius prolixus* nitrophorins (*Rp*-NPs) (25–27), human  $\alpha_1$ -microglobulin (*Hs*- $\alpha_1$ -m) (28, 29), *Cimex lectularius* nitrophorin (*Cl*-NP) (30), *Arabidopsis thaliana* nitrobindin (*At*-Nb) and *Homo sapiens* THAP4 (*Hs*-THAP4) (31–33).

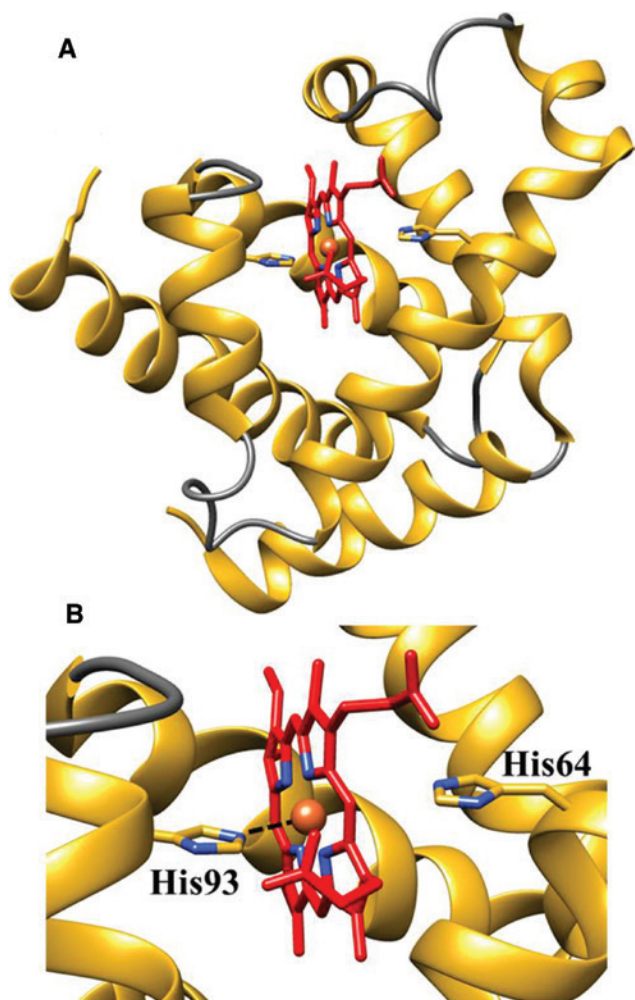


**Figure 1:** The three-dimensional structure of deoxygenated *Pc-Mb-Fe(II)*.

An overview (panel A; ID PDB code: 1VXB) and some details of the heme pocket (panel B; ID PDB code: 1VXB). The proximal His93 and the distal His64 residues are shown. This and the following figures have been drawn with UCSF-Chimera package (20).

*Rp*-NPs and *Hs- $\alpha_1$ -m* are eight-stranded anti-parallel all  $\beta$ -barrel heme-proteins belonging to the lipocalin family (25, 27). *At-Nb* and *Hs-THAP4* display a ten-stranded anti-parallel all  $\beta$ -barrel fold could be considered as the heme-binding prototypes of the Nb family (31, 32). *Cl*-NP displays a mixed  $\alpha$ -helical- $\beta$ -barrel fold, being structurally related to bacterial exonuclease III (34) and to human inositol polyphosphate-5-phosphatase (30, 35). In *Rp*-NPs, *Hs- $\alpha_1$ -m* and Nbs, the penta-coordinated heme-Fe atom is tethered to the protein by the imidazole ring of the proximal His residue, which is replaced by the Cys side chain in *Cl*-NP. The heme distal His residue, present in most of all  $\alpha$ -helical globins, is absent in NPs, *Hs- $\alpha_1$ -m* and Nbs avoiding heme-Fe hexa-coordination and, in turn, causes the loss of the metal center reactivity. Moreover, the high

solvent exposure of the heme does not permit the reduction of the heme Fe-atom, which is stable in the ferric form. This allows to selectively bind small neutral and anionic molecules (e.g. NO) (36, 37).

The structural organization of all  $\alpha$ -helical globins, binding the ferrous heme-Fe and of all  $\beta$ -barrel and mixed  $\alpha$ -helical- $\beta$ -barrel heme-proteins, joining the ferric heme-Fe, is at the root of their different functions (30, 31, 38). Here, the structural and functional properties of Nbs, *Hs- $\alpha_1$ -m* and NPs are examined in parallel with those of sperm whale (*Physeter catodon*) myoglobin (*Pc-Mb*), which is generally taken as the molecular model of monomeric globins (39).

## Heme-binding lipocalins

The lipocalins form a widespread superfamily of single domain extracellular proteins described in bacteria, plants, invertebrate and vertebrates (40–42). They are characterized by a large cup-shaped  $\beta$ -barrel structure that contains eight anti-parallel  $\beta$ -strands able to bind small hydrophobic molecules, including the heme, as well as exogenous molecules (40, 41, 43). Although for a long time, it was thought that *Rp*-NPs were the only lipocalins able to bind heme, in 2012, *Hs- $\alpha_1$ -m* has been reported to host the heme and to participate in heme metabolism (44).

## Nitrophorins

The nitrophorins (NPs) represent a group of NO-carrying heme proteins identified for the first time in the salivary glands of *Rp*. (26, 45). *Rp*-NPs possess anti-hemostatic activity, storage, transport and release of NO and binds host histamine (26, 27, 37). Of note, *Rp*-NPs are synthesized in the salivary glands where NO is produced from a NO-synthase similar to mammalian constitutive isoforms (46). Although not evolutionarily related to *Rp*-NPs, the *Cl*-NP also transports, stores and releases NO by using a ferric heme-Fe. As expected from the high sequence divergence among lipocalins, the shape of the  $\beta$ -barrel, the positioning of the hydrophobic ligands in the barrel core and the loops lining the barrel entrance are very different in NPs (30, 47, 48).

## *Rhodnius prolixus* nitrophorins

About 6 million people worldwide, mostly in Latin America, are estimated to be affected by Chagas disease,

which is caused by *Trypanosoma cruzi* (49, 50). *Trypanosoma cruzi* is mainly transmitted by contact with the feces/urine of infected hematophagous Triatominae insects like *Rp* (51), which typically lives in the wall or roof cracks of poorly-constructed homes in rural or suburban areas. Chagas disease is characterized by two phases: the initial and acute phase, in which, a high number of parasites circulate in the blood but during which symptoms are absent or mild, and the late and chronic phase, in which the parasites infest the heart and the digestive tract muscles. Most of the patients affected by Chagas disease suffer from cardiac, gastrointestinal, neurological, or mixed disorders. In later years, the infection can lead to death by progressive destruction of the heart and its conducting fibers (49).

The saliva of *Rp* contains several proteins including: (i) three platelet aggregation inhibitors (named from RPAI1 to RPAI3) (52); (ii) an anti-thrombin protein that modulates the blood-pumping frequency, facilitating the feeding efficiency of Triatominae (53, 54); (iii) six *Rp*-NPs (designated from *Rp*-NP1 to *Rp*-NP6) that induce the vasodilation releasing NO and impair the activation of the host inflammation and immune responses by trapping histamine; (iv) *Rp*-NP2, also called prolixin-S, which blocks both the intrinsic and extrinsic coagulation pathways by inhibiting the factor IX (55, 56); and (v) *Rp*-NP7 that is devoted to impair platelet aggregation (26, 27, 37). Although *Rp*-NPs have been extensively studied and are structurally well characterized, it remains a matter of debate why *Rp* uses a set of NPs.

The *Rp*-NPs family arose from gene duplication as indicated by the very high amino acid sequence identity between NP1 and NP4 and between NP2 and NP3 (26). Among the seven *Rp*-NPs so far identified, the crystal structure has been solved for *Rp*-NP1, *Rp*-NP2, *Rp*-NP4 and *Rp*-NP7 (37, 57–59). The *Rp*-NPs are ~20 kDa proteins showing a common fold characterized by eight anti-parallel  $\beta$ -strands, three short  $\alpha$ -helices and two disulfide bridges (Figure 2) (26, 37, 57–60). Of note, the position of the Cys residues forming the disulfide bonds is conserved among other insect-derived lipocalins such as bilin binding protein and insecticyanin (40, 61).

In *Rp*-NPs, the heme is located in one end of the  $\beta$ -barrel and is bound to the protein by the proximal His residue (25, 57, 61). The heme is surrounded by ten hydrophobic residues in addition to the proximal His (i.e. His57 in *Rp*-NP2, *Rp*-NP3 and *Rp*-NP7; and His59 in *Rp*-NP1 and *Rp*-NP4) that represents the 5th heme-Fe ligand. The distal His residue, present in most globins, is absent in *Rp*-NPs. The heme contacts the Leu123 and Leu133 residues with a distance of ~3.4 Å from both of them (Figure 2). This

packing results in a highly non-planar and distorted heme in which the four pyrroles are rotated out of the plane, giving rise to a ruffled heme (Figure 2) with altered electronic and chemical properties compared to the normal heme (26, 62–64).

NP7 is highly divergent from the other NPs due to the presence of 27 Lys residues (out of a total of 185 amino acid residues) that cluster at the surface opposite to the heme pocket (37, 60). This confers to *Rp*-NP7 a positive charge to bind membrane phospholipids (37, 59, 65).

In contrast to almost all  $\alpha$ -globins, the heme-Fe atom of *Rp*-NPs is in the ferric form; in fact, the values of the midpoint potential of the heme-Fe atom of NPs is ~300 mV more negative than those of Mb and Hb (66, 67). The Asp29 and Glu53 residues in the heme distal pocket of *Rp*-NPs are too far to coordinate the heme-Fe atom, but could contribute to the negative mid-point potential of the metal center (67). Accordingly, the introduction of a Glu or Asp residue in the heme distal pocket of *Pc*-Mb at position E7 decreases the value of the midpoint potential by ~200 mV (68). The negative values of the midpoint potential of the heme-Fe atom of *Rp*-NPs impair the reductive nitrosylation of the metal center (25, 58, 67, 69), in contrast to most of the  $\alpha$ -globins (66–68, 70).

Ligands bind to the heme distal site, which is part of a large and open cavity. In particular, NO is coordinated to the heme-iron of *Rp*-NP4 with a bond distance of 1.66 Å and a Fe-N-O angle of 156° that facilitates van der Waals contacts between NO and the Leu123, Leu130 and Leu 133 residues (Figure 2) (58, 63). The heme-Fe atom and the N and O atoms of NO are placed on the same plane of the proximal His ring. This is coherent with the Fe(III) oxidation state stabilized by the ruffled heme (58, 63).

Upon NO binding to *Rp*-NP4, the rotation of the pyrrole rings becomes more pronounced, the iron moves out of the pyrrole nitrogens plane and into the distal pocket by 0.06 Å and the heme becomes even more ruffled. Furthermore, this rotation causes the packing of the AB and GH loops around the NO to form a hydrophobic cavity (26, 27, 61, 63). NO protection within the *Rp*-NPs protein is necessary to prevent its reaction with solvent molecules such as O<sub>2</sub>, water, hydroxide, or thiols during storage and transport (25, 27). The different rates by which the AB and GH loops move in and out of the distal pocket upon NO association and dissociation are at the root of biphasic and triphasic processes, respectively (Table 1) (25, 58, 71).

Although NO binds to either ferrous or ferric heme-proteins, the kinetic parameters are very different (Table 1). Of note, the first-order dissociation rate constant for *Rp*-NP(III)-NO denitrosylation is faster by about 5-orders of magnitude than that of *Pc*-Mb(II)-NO (25, 67,

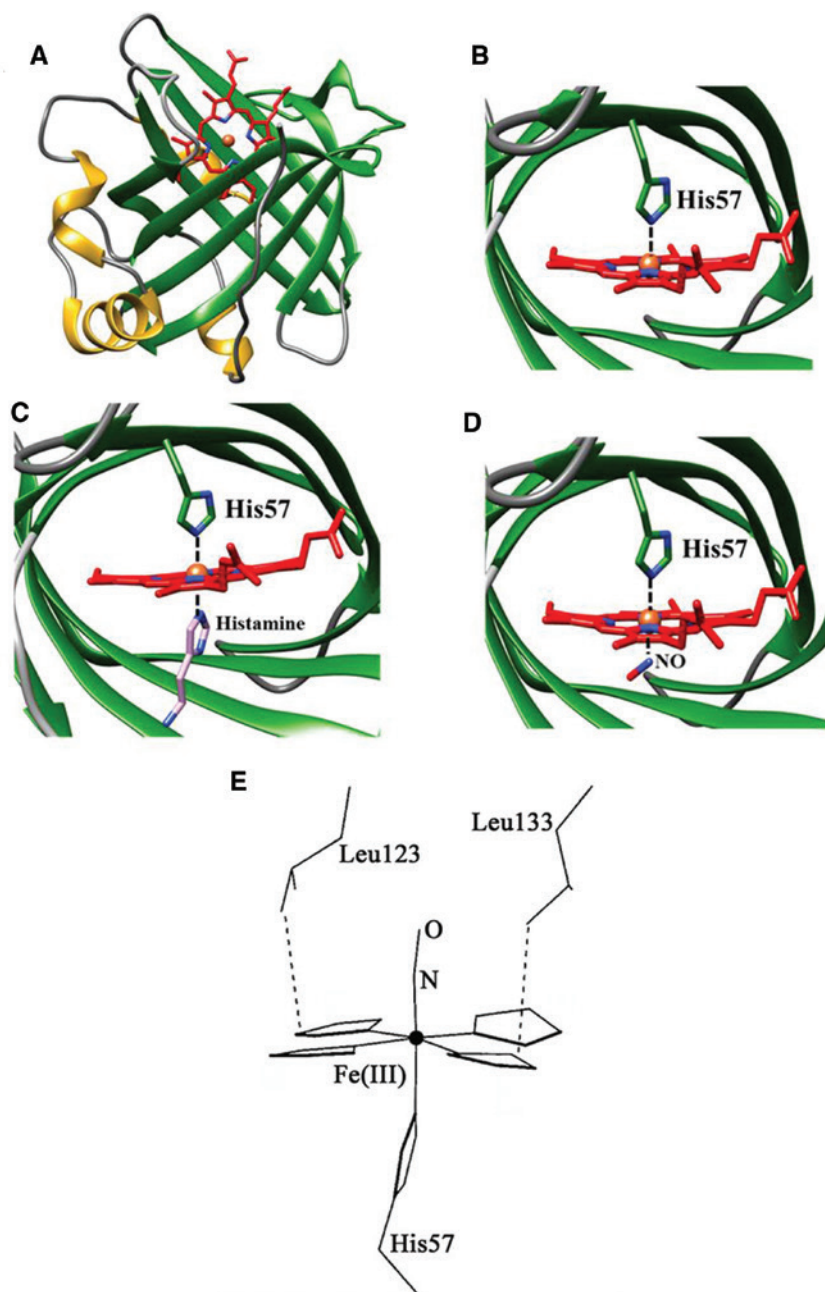


**Figure 2:** Three-dimensional structure of *Rp*-NP-Fe(III).

An overview (panel A; ID PDB code: 4XMC), details of the ligand-free heme pocket (panel B; ID PDB code: 4XMC), details of the histamine-bound derivative (panel C; ID PDB code: 4XMF) and details of the nitrosylated species (panel D; ID PDB code: 4XME). Packing of the Leu123 and Leu133 residues results in the ruffled heme of *Rp*-NP-Fe(III)-NO, as highlighted from the four pyrrole rings that are rotated out of the plane (panel E; modified from Ref. 62). In panel E, the non-pyrrole atoms have been omitted for clarity. The proximal His57 residue is shown.

70, 75, 76) to easily release NO in the host tissues during blood-sucking of Triatominae (25, 58, 67).

NO release in the host tissues is a pH-driven process (25, 27, 30, 77). Indeed, while in the insect salivary glands, the pH ranges between 5.0 and 5.5, in the host tissues it is ~7.3. *Rp*-NPs modulate NO release by shifting from the ‘closed’ conformation at low pH value, to the ‘open’

state at neutral pH. In the closed conformation, the AB and GH loops, which are positioned at the heme side of the barrel, are collapsed on the heme and prevent NO release. In *Rp*-NP2 and *Rp*-NP4, the pH-dependent conformational change is caused by the deprotonation of the Asp29 and Asp30 residues, respectively (78). Indeed, upon pH increase in the blood of the victim, the

**Table 1:** Kinetic and thermodynamic parameters for ligand binding to *Rp*-NPs, *At*-Nb and *Pc*-Mb.<sup>a</sup>

Protein	Ligand	$k'_1$ (/M/s)	$k'_2$ (/s)	$k_1$ (/s)	$k_2$ (/s)	$k_3$ (/s)	$K_1 = k'_1/k_1$ (/M)
<i>Rp</i> -NP1-Fe(III) <sup>b</sup>	NO	$1.5 \times 10^6$		4.3		$6.0 \times 10^{-1}$	$3.5 \times 10^5$
<i>Rp</i> -NP2-Fe(III) <sup>c</sup>	NO	$6.8 \times 10^6$	$\sim 2.5 \times 10^1$	$2.7 \times 10^1$			$2.5 \times 10^5$
<i>Rp</i> -NP2-Fe(III) <sup>b</sup>	NO	$3.3 \times 10^7$	$\sim 4.2 \times 10^1$	$3.2 \times 10^1$	$1.2 \times 10^{-1}$	$1.0 \times 10^{-2}$	$1.0 \times 10^6$
<i>Rp</i> -NP3-Fe(III) <sup>b</sup>	NO	$6.7 \times 10^6$	$\sim 3.3 \times 10^1$	$3.0 \times 10^1$	$8.0 \times 10^{-2}$	$1.0 \times 10^{-2}$	$2.2 \times 10^5$
<i>Rp</i> -NP4-Fe(III) <sup>d</sup>	NO	$2.5 \times 10^6$	$3.2 \times 10^1$	$1.5 \times 10^1$	1.8	$6.0 \times 10^{-1}$	$1.7 \times 10^5$
<i>At</i> -Nb-Fe(III) <sup>e</sup>	NO	$1.2 \times 10^6$		$7.3 \times 10^1$			$1.6 \times 10^4$
<i>Pc</i> -Mb-Fe(III) <sup>f</sup>	NO	$7.0 \times 10^4$		$1.2 \times 10^1$			$6.7 \times 10^3$
<i>At</i> -Nb-Fe(II) <sup>e</sup>	NO	$8.1 \times 10^7$		$\sim 8 \times 10^{-2}$			$\sim 1 \times 10^9$
<i>Pc</i> -Mb-Fe(II) <sup>f</sup>	NO	$2.2 \times 10^7$		$9.8 \times 10^{-5}$			$2.2 \times 10^{11}$
<i>Rp</i> -NP4-Fe(II) <sup>g</sup>	CO	$7.9 \times 10^6$					
<i>At</i> -Nb-Fe(II) <sup>e</sup>	CO	$2.3 \times 10^5$		$5.0 \times 10^{-2}$			$4.5 \times 10^6$
<i>Pc</i> -Mb-Fe(II) <sup>h</sup>	CO	$5.1 \times 10^5$		$1.9 \times 10^{-2}$			$2.7 \times 10^7$
<i>Rp</i> -NP1-Fe(III) <sup>b</sup>	Histamine	$4.3 \times 10^6$					
<i>Rp</i> -NP2-Fe(III) <sup>c</sup>	Histamine	$4.6 \times 10^6$	$\sim 1.2 \times 10^1$	$1.4 \times 10^1$			$3.3 \times 10^5$
<i>Rp</i> -NP2-Fe(III) <sup>b</sup>	Histamine	$1.0 \times 10^7$	$\sim 3.1 \times 10^1$	$1.6 \times 10^1$			$6.3 \times 10^5$
<i>Rp</i> -NP3-Fe(III) <sup>b</sup>	Histamine	$6.8 \times 10^6$	$\sim 1.5 \times 10^1$	$1.3 \times 10^1$			$5.2 \times 10^5$
<i>Rp</i> -NP4-Fe(III) <sup>d</sup>	Histamine	$4.7 \times 10^6$	$2.0 \times 10^1$				

<sup>a</sup> $k'$  indicates the second order rate constant for ligand binding to heme-Fe,  $k$  indicates the first order rate constant for ligand dissociation from heme-Fe and  $K$  indicates the dissociation equilibrium constant for ligand binding to heme-Fe. The subscripts 1, 2 and 3 indicate the kinetic and thermodynamic parameters of the first, the second and the third step of ligand binding to and dissociation from heme-Fe, respectively.

<sup>b</sup>pH 8 and 25°C. From (25).

<sup>c</sup>pH 8 and 12°C. From (25).

<sup>d</sup>pH 8 and 25°C. From (71).

<sup>e</sup>pH 7 and 20°C. From (31).

<sup>f</sup>pH 7 and 20°C. From (72–74).

<sup>g</sup>pH 8 and room temperature. From (58).

<sup>h</sup>pH 7 and 20°C. From (23).

Asp29-Leu132 hydrogen bond in *Rp*-NP2 and the Asp30-Leu130 hydrogen bond in *Rp*-NP4 break down, the newly charged Asp residues become solvated and the transition to the open conformation takes place with the consequent NO release (78, 79). Subsequently NO binds to the host soluble guanylate cyclase protein causing smooth muscle relaxation and vasodilation (80, 81).

Once in the host, *Rp*-NP-Fe(III) traps the histamine released from platelets and mast-cells to prevent the re-association of NO and to impair the activation of the host inflammation and immune responses. Indeed, upon histamine scavenging, the itching response deriving from the recognition of salivary antigens by the host IgE is limited (26, 37, 67, 82).

Histamine is coordinated to the heme iron through the Nε2 of its imidazole ring, the angle between the imidazole ring and the heme proximal His (i.e. His59 in *Rp*-NP1 and *Rp*-NP4; His57 in *Rp*-NP2, *Rp*-NP3 and *Rp*-NP7) being approx. 32°. The *Rp*-NP1:histamine complex is stabilized by hydrogen bonds that occur between the Asp30 and Glu32 residues of *Rp*-NP1 and the alkylammonium group of histamine (Figure 2) (57). The same

heme-Fe(III)-histamine geometry occurs also in *Rp*-NP4 and *Rp*-NP7 (37, 63).

Kinetic parameters for NO and histamine binding to *Rp*-NP1-Fe(III), *Rp*-NP2-Fe(III), *Rp*-NP3-Fe(III) and *Rp*-NP4-Fe(III) are closely similar. At variance with *Rp*-NP-Fe(III)-NO denitrosylation, the dissociation of the *Rp*-NP-Fe(III)-histamine complex is a monophasic process, reflecting the open conformation of the heme distal pocket (Table 1) (25, 71) (Table 1).

Under anaerobic conditions (i.e. in the presence of sodium dithionite) *Rp*-NP4-Fe(II) reacts quickly with CO, the value of  $k'_1$  ( $=7.9 \times 10^6$ /M/s) for *Rp*-NP4-Fe(II) carbonylation (58) being higher by about one order of magnitude than that for CO binding to *Pc*-Mb-Fe(II)  $k'_1$  ( $=5.1 \times 10^5$ /M/s) (Table 1) (23). This possibly reflects the different proximal His-heme-Fe geometry of all-α and all-β heme-proteins (7, 58).

Overall, understanding the mechanisms of infection of *Rp* may help in the proper treatment of patients affected by Chagas disease as well as in understanding the insecticide resistance processes (83). In this context, *Rp*-NPs represent prototypic proteins required to study the molecular

mechanism underpinning the interaction between the host and the parasite.

### *Cimex lectularius* nitrophorin

*Cimex lectularius* (*Cl*) is a hematophagous insect known as a human and domestic animal parasite (84, 85). In the second half of the 20th century, the use of pesticides significantly decreased the spread of *Cl* in Europe (86). However, it has been recently reported that a dramatic increase of the diffusion of this parasite has occurred due to the higher incidence of international travel, immigration and insecticide resistance (85, 87). Although many disease pathogens have been reported in *Cl*, the latter may possess ‘neutralizing factors’ that attenuate pathogen virulence and thereby, decrease the ability of bed bugs to transmit infectious disease. However, *Cl* has been recently reported to be a competent vector for *Bartonella quintana* and *T. cruzi*, the causes of trench fever and Chagas disease, respectively (88).

*Cl* expresses a single NP (*Cl*-NP) structurally different from *Rp*-NPs although sharing similar biological functions, such as NO storage, transport and release (30, 47, 48). In fact, *Cl*-NP is structurally homologous to a bacterial exonuclease (34) and to the human inositol polyphosphate-5-phosphatase (35, 48).

The *Cl*-NP transcript is an open reading frame of 906 base pairs (bp) that codes for a precursor protein of 302 amino acids. The secreted protein usually contains a signal peptide that is lost upon cleavage of the Ala20-Gly21 bond. The processed protein consists of 282 amino acids with a molecular mass of ~30 kDa (48).

The three-dimensional (3D) structure of *Cl*-NP consists of an extensive  $\beta$ -sandwich motif characterized by 11 anti-parallel  $\beta$ -strands and three  $\alpha$ -helices connected to the  $\beta$ -barrel by loops (Figure 3) (30). The *Cl*-NP contains: (i) two potential glycosylation sites placed within the Asn122-Glu123-Thr124-Ile125 and Asn199-Ala200-Thr201-His202 regions, (ii) several protein kinase C phosphorylation sites characterized by the Thr-Xxx-Lys, Thr-Xxx-Arg and Ser-Xxx-Lys consensus sequences and (iii) a potential *N*-myristylation site within the Gly136-Gly137-Ile138-Val139-Thr140-Ser141 sequence (30).

The heme-Fe is hosted in a hydrophobic pocket above one face of the sandwich. The sulfur atom of Cys60 represents the 5th coordination bond of the heme-Fe atom, which is located near the *N*-terminus of the proximal  $\alpha$ -helix (Figure 3). The Cys60 residue is also hydrogen bonded to the Gln56 residue, this bond possibly strengthening NO binding. The heme is moderately ruffled, with

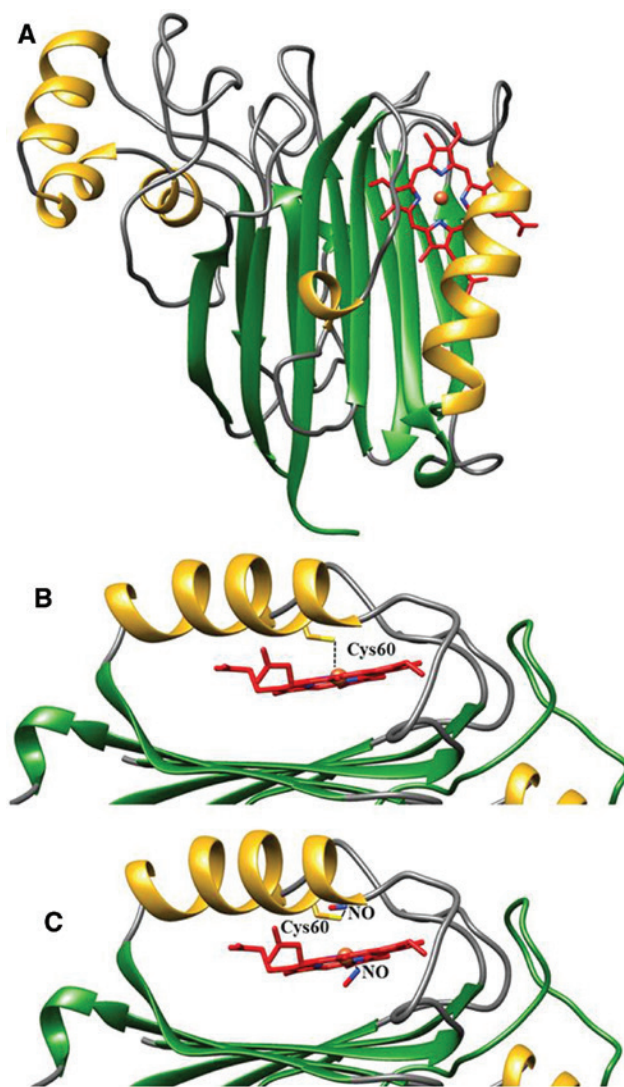


**Figure 3:** Three-dimensional structure of *Cl*-NP-Fe(III). An overview (panel A; ID PDB code: 2IMQ), details of the ligand-free heme pocket (panel B; ID PDB code: 2IMQ) and details of the nitrosylated species (panel C; ID PDB code: 1Y21). The proximal Cys60 residue is shown.

the heme-Fe shifted 0.36 Å out of the heme plane towards the proximal Cys60 residue. The *Cl*-NP distal pocket is small and hydrophobic (35 Å<sup>3</sup>) and contains three solvent molecules, one of which is weakly associated with the heme-Fe (30).

In contrast to *Rp*-NPs, *Cl*-NP does not bind histamine but rather binds reversibly two molecules of NO. The diatomic gaseous ligand first binds to the heme-Fe(III) atom, leading to the formation of the penta-coordinated heme-Fe(II)-NO adduct. In the presence of an excess of NO, the diatomic gas reacts with the Cys60 thiolate leading to the formation of a neutral *S*-nitrosyl (SNO) conjugate. In the presence of low levels of NO or increased pH values, NO

dissociates from *Cl*-NP by reversal steps. The dissociation of the Cys60-SNO adduct is facilitated by electron transfer from the heme-Fe(II)-NO adduct to the Cys60-S atom. In parallel, the heme-Fe(II)-NO adduct is converted to the heme-Fe(III)-NO complex, which releases quickly the diatomic gas (30, 89).

The (de)nitrosylation mechanism and structure of *Cl*-NP are completely different from those of the *Rp*-Nps, highlighting the divergent evolution of proteins involved in the insects' blood feeding (26, 27, 30, 37, 45).

## Human $\alpha_1$ -microglobulin

*Hs- $\alpha_1$ -m* (also known as protein HC, 'human complex forming protein, heterogeneous in charge') has a wide phylogenetic distribution, being well conserved among vertebrates (28, 90). The  $\alpha_1$ -microglobulin/bikunin precursor *AMBP* human gene, which maps to a lipocalin gene cluster in the 9q32-22 region in humans (91), encodes for a precursor that is splitted into *Hs- $\alpha_1$ -m* and bikunin, a proteinase inhibitor and component of the extracellular matrix (92, 93). The *Hs- $\alpha_1$ -m*/bikunin precursor is expressed mainly in the liver and after its cleavage, the two mature proteins are secreted separately into the bloodstream (90, 94). *Hs- $\alpha_1$ -m* has been found expressed in most tissues, in the interstitial fluids and in plasma (94–96), where about 50% of it forms a 1:1 complex with the plasmatic immunoglobulin A (IgA) (97).

Plasma *Hs- $\alpha_1$ -m* is involved in heme transport and extracellular clearance (28). Moreover, *Hs- $\alpha_1$ -m* protects cells and tissues against oxidative waste products and transports them to the kidneys for degradation and/or excretion (96). The anti-oxidative protection of *Hs- $\alpha_1$ -m* is achieved by its reductase and radical-binding activities exerted through the Cys34 unpaired thiol group and the side-chains of the Lys92, Lys118 and Lys130 residues (98–100). Of note, a truncated form of *Hs- $\alpha_1$ -m* lacking the C-terminal tetrapeptide, called t-*Hs- $\alpha_1$ -m*, has been found in human urine, skin and placenta. This truncated form not only maintains the capability to bind the heme, but also induces its degradation (29, 101, 102).

*Hs- $\alpha_1$ -m* is a heterogeneously charged glycoprotein of 26 kDa composed of 183 amino acids (92), the glycosylation sites being at the Thr5, Asn17 and Asn96 residues (103). *Hs- $\alpha_1$ -m* shows the typical kernel lipocalin  $\beta$ -barrel fold that is open to the solvent at one end and is characterized by eight anti-parallel  $\beta$ -strands (labeled as A–H) connected by four structurally variable loops (designated as 1–4) connecting pairs of neighboring  $\beta$ -strands (40, 41, 104). Loop 1 includes a short  $\alpha$ -helix that closes

one end of the barrel and the Cys34-Pro35 dyad that binds the heme-Fe. Loop 2 connects the  $\beta$ -strands C and D. Loop 3 connects the  $\beta$ -strands B and C that are placed at the closed bottom of the  $\beta$ -barrel. Loop 4 contains a Ni<sup>2+</sup>-binding site (104). The Cys72-Cys169 disulfide bond links the C-terminal region to the region between loop 2 and the  $\beta$ -strand D, which represents a conserved structural feature of the lipocalin family (105). The Lys118 and Lys92 residues pave the top region of the *Hs- $\alpha_1$ -m* central cavity, which is wider than in most lipocalins, while Lys130 residue is positioned halfway down towards the bottom of the cavity. Cys34, Met62, Met99, Lys118 and Lys130 residues are involved in ligand recognition (104, 106, 107), although none of them are conserved among orthologous *Hs- $\alpha_1$ -m* species (104). Residues Arg43, Arg66, Arg68, Lys69, Lys92, Lys94, Lys118 and Lys130 line the upper part of the pocket, whereas the hydrophobic side chains of the Tyr79, Phe88, Phe114 and Tyr132 residues form the lower cavity of the pocket. These hydrophobic residues form  $\pi$ -stacking interactions and contribute to ligand binding. Overall, the positive potential inside the *Hs- $\alpha_1$ -m* cavity and the non-polar environment at the bottom of the pocket allow preferential binding of negatively charged ligands with hydrophobic moiety(ies) (Figure 4) (104).

*Hs- $\alpha_1$ -m* binds the heme-Fe with *K* values ranging between  $1 \times 10^5/\text{M}$  and  $1 \times 10^6/\text{M}$  (28, 101, 102, 108). Moreover, values of *K'* and *k* for heme-Fe binding to *Hs- $\alpha_1$ -m* are  $5.7 \times 10^2/\text{M/s}$  and  $7.7 \times 10^{-3}/\text{s}$ , respectively (108). Structural, spectroscopic and functional evidence supports the view that the *Hs- $\alpha_1$ -m*:heme stoichiometry is 1:2 (44, 104, 108). The main binding site has been hypothesized to be located in the lipocalin pocket (108), the second cleft being placed between loops 1 and 4 at the outer rim of the pocket (Figure 4) (104, 108). In the inner pocket, the non-pyrrolic groups of the heme-Fe have been suggested to be in close proximity with the Lys118 and Lys130 residues. These residues may react with the inner heme-Fe group leading to the covalent attachment of the degradation products (108). In the outer cleft, the Cys34 and His123 residues coordinate the heme-Fe atom (104, 108). Of note, the inner and outer sites are filled in that order by increasing the heme-Fe concentration (108).

As observed in several lipocalins (40, 41, 96, 104), the Cys34 residue of *Hs- $\alpha_1$ -m* is involved in the IgA covalent binding (109). However, the affinity of heme-Fe for the *Hs- $\alpha_1$ -m*:IgA complex ( $K = 2 \times 10^5/\text{M}$ ) is similar to that for the heme-Fe recognition by free *Hs- $\alpha_1$ -m*. Therefore, heme-Fe binds the *Hs- $\alpha_1$ -m*:IgA complex in the inner pocket (28, 110). Therefore, IgA should not affect the macrocycle degradation.

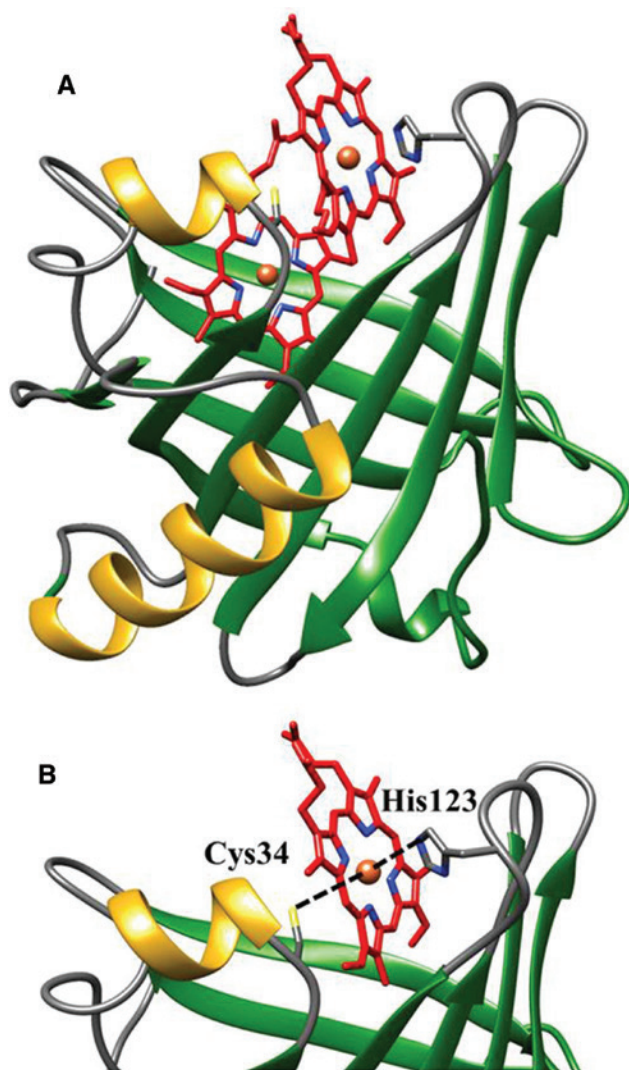


**Figure 4:** Three-dimensional structure of *Hs-α<sub>1</sub>-m*. An overview (panel A; ID PDB code: 3QKG) and some details of the hypothetical binding modes of the two heme groups (panel B). The two heme groups were positioned according to literature data (104). The proximal His123 and the distal Cys34 residues are shown.

## Nitrobindins

In 2010, heme binding has been reported to occur in a fatty acid-binding protein (FABP)-like protein expressed in *At* and named nitrobindin (*At-Nb*) (31). Although Nbs have been identified in different species and show a ‘FABP-like’ ten-stranded  $\beta$ -barrel fold, they (i) possess cross-barrel electrostatic interactions that are absent in FABPs and (ii) do not show the two  $\alpha$ -helices followed by a hairpin on the opposite side of the barrel that are present in FABPs (33). Moreover, the phylogenetic tree reconstruction indicates that Nbs and FABPs cluster separately, Nbs forming a ubiquitous heme-protein family spanning from

bacteria to *Hs* (33). All the Nb-like proteins display conserved residues in the pocket involved in the coordination and recognition of the heme-Fe. Moreover, molecular models of putative Nbs from different organisms match very well with the 3D structure of *At-Nb* and of the human homolog of *At-Nb* [i.e. human thanatos-associated protein 4 (THAP4)] (33).

The gene coding for *At-Nb* (i.e. *AT1G79260*) is located on chromosome 1 and is composed of four exons (111). The *At-Nb* transcript is composed of 542 bp and codes for a 166 amino acids protein displaying a 3D structure composed of ten-stranded  $\beta$ -barrel (Figure 5).

The *N*-terminal  $3_{10}$  helix of *At-Nb* closes the hydrophobic core of the protein and is stabilized by hydrogen bonds between the Trp30 side chain and the backbone carbonyl group of the Leu26 residue and between the Lys165 side chain and the carbonyl groups of Tyr25 and Leu27 residues (33). The central part of the  $\beta$ -barrel of *At-Nb* is stabilized by two salt bridges between Arg133 and the carboxylate groups of Glu78 and Glu102 and by two strong hydrogen bonds between Tyr144 and Glu48 and between Glu78 and Tyr62 (33) (Figure 5). The heme pocket of *At-Nb* is relatively open and exposed to the solvent and interacts with the protein moiety by multiple van der Waals interactions. The proximal His158 and the distal His76 side chains face the heme, although His76 seems to be located too far away from the heme-Fe atom to properly coordinate it (31).

The exposure of the *At-Nb* heme-Fe may be at the root of: (i) the high value of the heme-Fe(III) dissociation rate from *At-Nb* heme-Fe(III) ( $=3.6 \times 10^{-5}/s$ ), which is one-order of magnitude larger than that of *Pc-Mb-Fe*(II), and (ii) the very high value of the  $O_2$ -dependent oxidation rate of the metal center of *At-Nb-Fe*(II) ( $1.0 \times 10^{-1}/s$ ), which is 10 000-fold larger than that of *Pc-Mb-Fe*(II) (1, 31, 112). These data suggest that the heme of *At-Nb* may be exchanged easily and is stably in the oxidized form in the presence of  $O_2$  (31). Accordingly, *At-Nb-Fe*(III) does not undergo reductive nitrosylation (31) as is observed in *Rp-NPs* (25, 58, 67, 69).

The value of  $K$  for NO binding to *At-Nb-Fe*(III) ( $1.6 \times 10^4/M$ ) (31) is 10-fold lower than those observed for *Rp-NP-Fe*(III) ( $\sim 2 \times 10^5/M$ ) (25, 71). Moreover, the nitrosylation rate constant of *At-Nb-Fe*(III) ( $k'_1 = 1.2 \times 10^6/M/s$ ) (31) is similar to those of *Rp-NP1-Fe*(III) ( $k'_1 = 1.5 \times 10^6/M/s$ ) (25) and *Rp-NP4-Fe*(III) ( $k'_1 = 2.5 \times 10^6/M/s$ ) (71), but higher than that of *Pc-Mb-Fe*(III) ( $k'_1 = 7.0 \times 10^4/M/s$ ) (72–74) (Table 1). The fast dissociation of NO from *At-Nb-Fe*(III)-NO ( $k = 7.3 \times 10^1/s$ ) (31) may be pivotal for NO metabolism (Table 1).

*At-Nb-Fe*(III) can be reduced by dithionite and bind NO and CO. The value of  $k'$  for *At-Nb-Fe*(II) nitrosylation

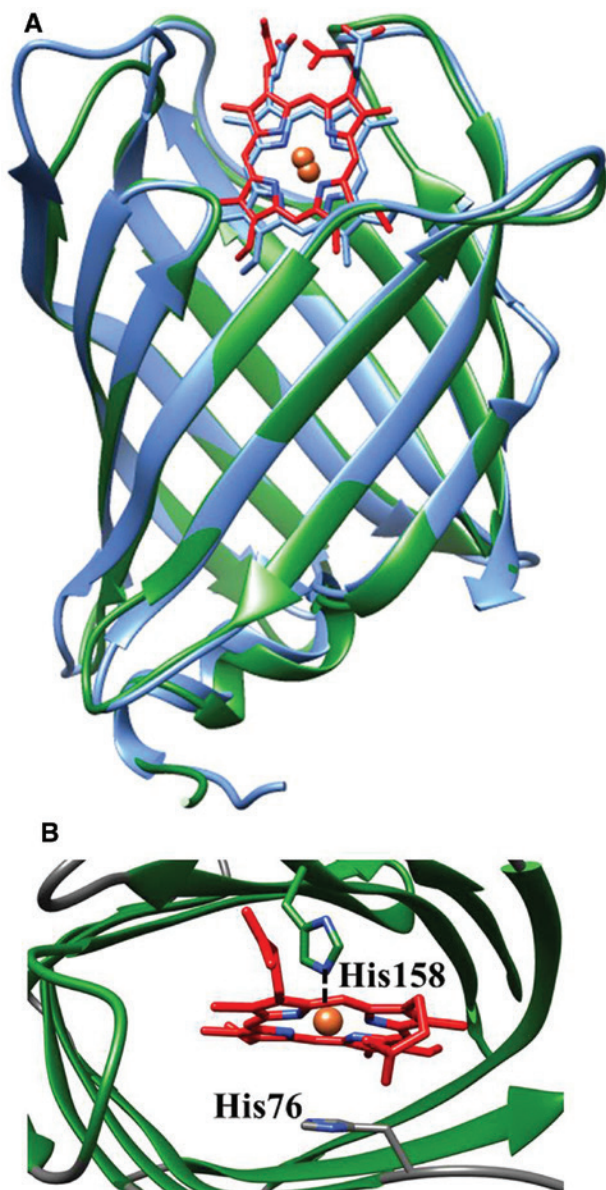


**Figure 5:** Superimposition of the three-dimensional structures of *At-Nb* (in green and red) and *Hs-Nb* (in blue) (panel A; ID PDB code: 3EMM and 3IA8, respectively) and some details of the ligand-free heme pocket of *At-Nb* (panel B; ID PDB code: 3EMM). The proximal His158 and the distal His76 residues are shown.

( $=8.1 \times 10^7/\text{M/s}$ ) exceeds by 4-folds that of *Pc-Mb-Fe(II)* ( $=2.2 \times 10^7/\text{M/s}$ ), whereas the value of  $k$  for *At-Nb-Fe(II)*-NO denitrosylation ( $\sim 8 \times 10^{-2}/\text{s}$ ) is faster by three-orders of magnitude than that of *Pc-Mb-Fe(II)*-NO ( $=9.8 \times 10^{-5}/\text{s}$ ). As a consequence, the affinity of NO for *At-Nb-Fe(II)* ( $K \sim 1 \times 10^9/\text{M}$ ) is lower than that of *Pc-Mb-Fe(II)* ( $=2.2 \times 10^{11}/\text{M}$ ) (31, 72–74) (Table 1). The value of  $k'$  for *Pc-Mb-Fe(II)* carbonylation ( $=5.1 \times 10^5/\text{M/s}$ ) exceeds by 2-folds that of CO binding to *At-Nb-Fe(II)* ( $=2.3 \times 10^5/\text{M/s}$ ),

whereas the value of  $k$  for *At-Nb-Fe(II)*-CO decarbonylation ( $5 \times 10^{-2}/\text{s}$ ) is faster by 2-folds than that of *Pc-Mb-Fe(II)*-CO ( $=1.9 \times 10^{-2}/\text{s}$ ). Thus, the affinity of CO for *At-Nb-Fe(II)* ( $K = 4.5 \times 10^6/\text{M}$ ) is lower than that of *Pc-Mb-Fe(II)* ( $=2.7 \times 10^7/\text{M}$ ) (23, 31) (Table 1). The low reactivity of *At-Nb-Fe(II)* has been hypothesized to reflect the proximal constraints limiting the in-to-out plane movement of the heme-Fe(II) atom (31).

The human THAP4 protein contains a human homolog of *At-Nb*. THAP4 consists of a *N*-terminal modified zinc finger domain, which has been proposed to bind DNA and of a *C*-terminus *At-Nb*-like domain, which could act as a NO sensor (32, 113, 114). It has been hypothesized that NO-binding to the *C*-terminal domain modulate the DNA binding activity of the *N*-terminal region, acting as an NO-dependent transcriptional regulator (31).

The exact role of Nbs is still unknown, although *At* produces NO in response to wounding and pathogenic infections. Therefore, it has been hypothesized that *At-Nb* may play a role in NO transport and release at the infection site and/or may rapidly reduce  $\text{O}_2$  to superoxide radicals with the generation of reactive oxygen species which, in turn, would represent a plant defense mechanism (31, 115–117).

## Therapeutic and biotechnological applications

The saliva of *Rp* has long been known to act as an anti-coagulant, this activity possibly residing in *Rp-NP2* and *Rp-NP7* (55, 56, 60, 65). *Rp-NP2* (also called prolixin-S) acts not only as a NO carrier but also in the blood coagulation cascade preventing the conversion of factor X to Xa (55, 56). Indeed, *Rp-NP2* is a good therapeutic molecule in the care of arterial thrombosis: 20–40  $\mu\text{g}/\text{ml}$  of *Rp-NP2* can reduce thrombin formation by 50%–80%, and 400  $\mu\text{g}/\text{kg}$  of *Rp-NP2* displays a better effect than heparin; furthermore, 1 mg/kg of *Rp-NP2* can even increase the time taken for carotid artery occlusion (56).

*Rp-NP7*, which is not devoted to NO storage and transport, displays a positively charged surface that enables it to bind to anionic phospholipid membranes. This process blocks the assembly of the pro-thrombinase complex on vesicles and activated platelets, inhibiting platelet aggregation (60, 65).

The rigid  $\beta$ -barrel scaffold of *At-Nb*, instead, provides a suitably sized cavity to host catalytic metal centers opening new avenues in the production of hybrid biocatalysts (118–120). A Rh complex with cyclopentadiene and

cyclooctadiene ligands has been synthesized as an artificial active site of *At*-Nb to catalyze the polymerization of phenylacetylene. The metal adduct has been covalently linked to the Cys96 residue of the Gln96Cys mutant of *At*-Nb by the maleimide group of cyclopentadiene which is tightly bound to Rh. *At*-Nb-Rh catalyzes preferentially the synthesis of *trans*-poly(phenylacetylene) (53%), whereas the Rh catalyst without the protein scaffold predominantly produces *cis*-poly(phenylacetylene) (93%). *At*-Nb-Rh has been reported to represent the unique example of biocatalyst inducing the C-C bond formation and the subsequent polymerization, which has never been seen in nature. This indicates that a rigid and chiral protein scaffold can function as a powerful platform for the modulation of monomer recognition during a propagation reaction (118, 121).

Also a  $(\mu\text{-S})_2\text{Fe}_2(\text{CO})_6$  complex was covalently embedded within the  $\beta$ -barrel of *At*-Nb to obtain a hydrogenase mode system. The  $(\mu\text{-S})_2\text{Fe}_2(\text{CO})_6$  complex is linked onto the *At*-Nb cavity by the dithiolate moiety with a maleimide group that forms a covalent bond with the Cys96 residue of the Gln96Cys mutant of *At*-Nb. *At*-Nb- $(\mu\text{-S})_2\text{Fe}_2(\text{CO})_6$  catalyzes the  $\text{H}_2$  production in a photocatalytic cycle based on the Ru-photosensitizer  $[\text{Ru}(2,2'\text{-bipyridine})_3]^{2+}$ . The *At*-Nb- $(\mu\text{-S})_2\text{Fe}_2(\text{CO})_6$  catalytic activity is slower than that of the  $(\mu\text{-S})_2\text{Fe}_2(\text{CO})_6$  complex lacking the protein matrix, probably reflecting the reduced accessibility of the Ru-photosensitizer to the diiron active site (119).

The terpyridine-(tpy) metal complexes catalyze a broad range of chemical reactions including cyclopropanation, cross coupling, benzylic oxygenation, olefin epoxidation and click reactions in combination with metal ions (122, 123). Recently, a hybrid biocatalyst containing a tpy-metal complex hosted in the cavity of *At*-Nb has been synthesized. The tpy was covalently linked to the Cys96 residue of the Gln96Cys/Met75Leu/Met148Leu/His76Leu/His158Leu mutant of *At*-Nb by the maleimide group of the maleimide-modified tpy. Although  $\text{Cu}^{2+}$ ,  $\text{Zn}^{2+}$  and  $\text{Co}^{2+}$  bind to the *At*-Nb-tpy complex, the *At*-Nb-tpy- $\text{Cu}^{2+}$  derivative catalyzes the Diels-Alder reaction between azachalcone and cyclopentadiene. The product yield is 2-fold higher than that of the tpy- $\text{Cu}^{2+}$  adduct without the protein. This suggests that *At*-Nb is a suitable scaffold for the design of the second coordination sphere of synthetic metal active sites (120).

## Conclusions

Small gases (i.e.  $\text{O}_2$ , CO,  $\text{CO}_2$ , NO,  $\text{NH}_3$  and  $\text{H}_2\text{S}$ ) participate in several biochemical processes in living cells. Thus,  $\text{CO}_2$  and  $\text{NH}_3$  regulate the acid-base homeostasis,

CO, NO and  $\text{H}_2\text{S}$  are involved in signaling and  $\text{O}_2$  is pivotal for metabolism. The reactive sites of these gases include metal centers (e.g. the heme) and active amino acids (e.g. Cys). Although  $\beta$ -barrel and mixed  $\alpha$ -helical- $\beta$ -barrel NPs, *Hs*- $\alpha_1$ -m and Nbs and all the  $\alpha$ -helical globins (e.g. Mb) host a heme group, the different structural organization and redox properties are at the root of their diverse functions. In fact, all  $\alpha$ -helical heme-proteins (e.g. Mb) host a ferrous heme-Fe whereas all  $\beta$ -barrel and mixed  $\alpha$ -helical- $\beta$ -barrel NPs, *Hs*- $\alpha_1$ -m and Nbs binds a ferric heme-Fe. Likely, the solvent-exposed ferric heme-Fe of NPs, *Hs*- $\alpha_1$ -m and Nbs plays a role in NO storage, transport and sensing whereas ferrous all  $\alpha$ -helical globins catalyze the  $\text{O}_2$ -based detoxification of the tight-bound NO. Lastly, all  $\beta$ -barrel heme-proteins may represent a frontline of anticoagulant strategies and a biotechnological frontier for the development of hybrid biocatalysts.

## List of abbreviations

<i>At</i>	<i>Arabidopsis thaliana</i>
<i>At</i> -Nb	<i>Arabidopsis thaliana</i> nitrobindin
bp	base pair
<i>Cl</i>	<i>Cimex lectularius</i>
<i>Cl</i> -Nb	<i>Cimex lectularius</i> nitrobindin
FABP	fatty acid binding protein
Hb	hemoglobin
<i>Hs</i>	<i>Homo sapiens</i>
<i>Hs</i> - $\alpha_1$ -m	<i>Homo sapiens</i> $\alpha_1$ -microglobulin
<i>Hs</i> -THAP4	<i>Homo sapiens</i> thanatos associated-protein 4 domain
IgA	plasmatic immunoglobulin A
Mb	myoglobin
Nb	nitrobindin
NP	nitrophorin
<i>Ps</i>	<i>Physeter catodon</i>
<i>Ps</i> -Mb	<i>Physeter catodon</i> myoglobin
<i>Rp</i>	<i>Rhodnius prolixus</i>
<i>Rp</i> -NP	<i>Rhodnius prolixus</i> nitrophorin
SNO	neutral S-nitrosyl
t- <i>Hs</i> - $\alpha_1$ -m	truncated <i>Hs</i> - $\alpha_1$ -m
tpy	terpyridine

**Acknowledgments:** The authors wish to thank Dr. Loris Leboffe (Interdepartmental Laboratory for Electron Microscopy, Roma Tre University, I-00146 Roma, Italy) for helpful discussions.

## References

1. Antonini E, Brunori M. Hemoglobin and myoglobin in their reactions with ligands. London, Amsterdam: North Holland Publishing Co, 1971.

2. Perutz MF. Regulation of oxygen affinity of hemoglobin: influence of structure of the globin on the heme iron. *Annu Rev Biochem* 1979; 48: 327–86.
3. Bunn HF, Forget BG. Hemoglobin: molecular, genetic and clinical aspects. Philadelphia: Saunders WB Company, 1986.
4. Ortiz de Montellano PR. Cytochrome P450: structure, mechanism, and biochemistry. Plenum: New York, 1995.
5. Olson JS, Phillips GN, Jr. Kinetic pathways and barriers for ligand binding to myoglobin. *J Biol Chem* 1996; 271: 17593–6.
6. Gray HB, Winkler JR. Electron transfer in proteins. *Annu Rev Biochem* 1996; 65: 537–61.
7. Bolognesi M, Bordo D, Rizzi M, Tarricone C, Ascenzi P. Nonvertebrate hemoglobins: structural bases for reactivity. *Prog Biophys Mol Biol* 1997; 68: 29–68.
8. Rodgers KR. Heme-based sensors in biological systems. *Curr Opin Chem Biol* 1999; 3: 158–67.
9. Chan MK. Recent advances in heme-protein sensors. *Curr Opin Chem Biol* 2001; 5: 216–22.
10. Smith LJ, Kahraman A, Thornton JM. Heme proteins-diversity in structural characteristics, function, and folding. *Proteins* 2010; 78: 2349–68.
11. Girvan HM, Munro AW. Heme sensor proteins. *J Biol Chem* 2013; 288: 13194–203.
12. Ascenzi P, Brunori M. A molecule for all seasons: the heme. *J Porphyrins Phthalocyanines* 2016; 20: 134–49.
13. Dickerson RE, Geiss I. The structure and action of proteins. New York, Evaston, London: Harper and Row Publishers, 1969.
14. Domingues-Hamdi E, Vasseur C, Fournier JB, Marden MC, Wajcman H, Baudin-Creuzat V. Role of  $\alpha$ -globin H helix in the building of tetrameric human hemoglobin: interaction with  $\alpha$ -hemoglobin stabilizing protein (AHSP) and heme molecule. *PLoS One* 2014; 9: e111395.
15. Vasseur C, Baudin-Creuzat V. Role of alpha-hemoglobin molecular chaperone in the hemoglobin formation and clinical expression of some hemoglobinopathies. *Transfus Clin Biol* 2015; 22: 49–57.
16. Pesce A, Couture M, Dewilde S, Guertin M, Yamauchi K, Ascenzi P, Moens L, Bolognesi M. A novel two-over-two  $\alpha$ -helical sandwich fold is characteristic of the truncated hemoglobin family. *EMBO J* 2000; 19: 2424–34.
17. Pesce A, Bolognesi M, Nardini M. The diversity of 2/2 (truncated) globins. *Adv Microb Physiol* 2013; 63: 49–78.
18. Takano T. Structure of myoglobin refined at 2.0 Å resolution: I. Crystallographic refinement of metmyoglobin from sperm whale. *J Mol Biol* 1977; 110: 537–68.
19. Takano T. Structure of myoglobin refined at 2.0 Å resolution: II. Structure of deoxymyoglobin from sperm whale. *J Mol Biol* 1977; 110: 569–84.
20. Pettersen EF, Goddard TD, Huang CC, Couch GS, Greenblatt DM, Meng EC, Ferrin TE. UCSF Chimera – a visualization system for exploratory research and analysis. *J Comput Chem* 2004; 25: 1605–12.
21. Kitagawa T, Ondrias MR, Rousseau DL, Ikeda-Saito M, Yonetani T. Evidence for hydrogen bonding of bound dioxygen to the distal histidine of oxycobalt myoglobin and haemoglobin. *Nature* 1982; 298: 869–71.
22. Olson JS, Mathews AJ, Rohlfs RJ, Springer BA, Egeberg KD, Sligar SG, Tame J, Renaud JP, Nagai K. The role of the distal histidine in myoglobin and haemoglobin. *Nature* 1988; 336: 265–6.
23. Rohlfs RJ, Mathews AJ, Carver TE, Olson JS, Springer BA, Egeberg KD, Sligar SG. The effects of amino acid substitution at position E7 (residue 64) on the kinetics of ligand binding to sperm whale myoglobin. *J Biol Chem* 1990; 265: 3168–76.
24. Brantley RE Jr, Smerdon SJ, Wilkinson AJ, Singleton EW, Olson JS. The mechanism of autooxidation of myoglobin. *J Biol Chem* 1993; 268: 6995–7010.
25. Andersen JF, Ding XD, Balfour C, Shokhireva TK, Champagne DE, Walker FA, Montfort WR. Kinetics and equilibria in ligand binding by nitrophorins 1–4: evidence for stabilization of a nitric oxide-ferriheme complex through a ligand-induced conformational trap. *Biochemistry* 2000; 39: 10118–31.
26. Montfort WR, Weichsel A, Andersen JF. Nitrophorins and related antihemostatic lipocalins from *Rhodnius prolixus* and other blood-sucking arthropods. *Biochim Biophys Acta* 2000; 1482: 110–8.
27. Andersen JF. Structure and mechanism in salivary proteins from blood-feeding arthropods. *Toxicon* 2010; 56: 1120–9.
28. Larsson J, Allhorn M, Åkerström B. The lipocalin  $\alpha_1$ -microglobulin binds heme in different species. *Arch Biochem Biophys* 2004; 432: 196–204.
29. Olsson MG, Centlow M, Rutardóttir S, Stenfors I, Larsson J, Hosseini-Maaf B, Olsson ML, Hansson SR, Åkerström B. Increased levels of cell-free hemoglobin, oxidation markers, and the antioxidative heme scavenger  $\alpha_1$ -microglobulin in preeclampsia. *Free Radic Biol Med* 2010; 48: 284–91.
30. Weichsel A, Maes EM, Andersen JF, Valenzuela JG, Shokhireva TK, Walker FA, Montfort WR. Heme-assisted S-nitrosation of a proximal thiolate in a nitric oxide transport protein. *Proc Natl Acad Sci USA* 2005; 102: 594–9.
31. Bianchetti CM, Blouin GC, Bitto E, Olson JS, Phillips Jr GN. The structure and NO binding properties of the nitrophorin-like heme-binding protein from *Arabidopsis thaliana* gene locus At1g79260.1. *Proteins* 2010; 78: 917–31.
32. Bianchetti CM, Bingman CA, Phillips Jr GN. Structure of the C-terminal heme-binding domain of THAP containing protein 4 from *Homo sapiens*. *Proteins* 2011; 79: 1337–41.
33. De Simone G, Ascenzi P, Polticelli F. Nitrobindin: an ubiquitous family of all  $\beta$ -barrel heme-proteins. *IUBMB Life* 2016; 68: 423–8.
34. Mol CD, Kuo CF, Thayer MM, Cunningham RP, Tainer JA. Structure and function of the multifunctional DNA-repair enzyme exonuclease III. *Nature* 1995; 374: 381–6.
35. Ross TS, Jefferson AB, Mitchell CA, Majerus PW. Cloning and expression of human 75-kDa inositol polyphosphate-5-phosphatase. *J Biol Chem* 1991; 266: 20283–9.
36. Shokhireva TK, Berry RE, Uno E, Balfour CA, Zhang H, Walker FA. Electrochemical and NMR spectroscopic studies of distal pocket mutants of nitrophorin 2: stability, structure, and dynamics of axial ligand complexes. *Proc Natl Acad Sci USA* 2003; 100: 3778–83.
37. Knipp M, Ogata H, Soavi G, Cerullo G, Allegri A, Abbruzzetti S, Bruno S, Viappiani C, Bidon-Chanal A, Luque FJ. Structure and dynamics of the membrane attaching nitric oxide transporter nitrophorin 7. *F1000Res* 2015; 4: 45.
38. Knipp M, He C. Nitrophorins: nitrite disproportionation reaction and other novel functionalities of insect heme-based nitric oxide transport proteins. *IUBMB Life* 2011; 63: 304–12.
39. Frauenfelder H, McMahon BH, Fenimore PW. Myoglobin: the hydrogen atom of biology and a paradigm of complexity. *Proc Natl Acad Sci USA* 2003; 100: 8615–7.
40. Flower DR. The lipocalin protein family: structure and function. *Biochem. J.* 1996; 318: 1–14.

41. Flower DR, North AC, Sansom CE. The lipocalin protein family: structural and sequence overview. *Biochim Biophys Acta* 2000; 1482: 9–24.
42. Schlehuber S, Skerra A. Lipocalins in drug discovery: from natural ligand-binding proteins to “anticalins”. *Drug Discov Today* 2005; 10: 23–33.
43. di Masi A, Trezza V, Leboffe L, Ascenzi P. Human plasma lipocalins and serum albumin: plasma alternative carriers? *J Control Release* 2016; 228: 191–205.
44. Siebel JF, Kosinsky RL, Åkerström B, Knipp M. Insertion of heme b into the structure of the Cys34-carbamidomethylated human lipocalin  $\alpha_1$ -microglobulin: formation of a [(heme)<sub>2</sub>( $\alpha_1$ -microglobulin)]<sub>3</sub> complex. *Chembiochem* 2012; 13: 879–87.
45. Walker FA, Ribeiro JM, Montfort WR. Novel nitric oxide-liberating heme proteins from the saliva of bloodsucking insects. *Met Ions Biol Syst* 1999; 36: 621–63.
46. Yuda M, Hirai M, Miura K, Matsumura H, Ando K, Chinzei Y. cDNA cloning, expression and characterization of nitric-oxide synthase from the salivary glands of the blood-sucking insect *Rhodnius prolixus*. *Eur J Biochem* 1996; 242: 807–12.
47. Valenzuela JG, Walker FA, Ribeiro JM. A salivary nitrophorin (nitric-oxide-carrying hemoprotein) in the bedbug *Cimex lectularius*. *J Exp Biol* 1995; 198: 1519–26.
48. Valenzuela JG, Ribeiro JM. Purification and cloning of the salivary nitrophorin from the hemipteran *Cimex lectularius*. *J Exp Biol* 1998; 201: 2659–64.
49. Hotez PJ, Bottazzi ME, Franco-Paredes C, Ault SK, Periago MR. The neglected tropical diseases of Latin America and the Caribbean: a review of disease burden and distribution and a roadmap for control and elimination. *PLoS Negl Trop Dis* 2008; 2: e300.
50. Schofield CJ, Galvão C. Classification, evolution, and species groups within the Triatominae. *Acta Tropica* 2009; 110: 88–100.
51. Parra-Henao G, Suárez-Escudero LC, González-Caro S. Potential Distribution of Chagas disease vectors (Hemiptera, Reduviidae, Triatominae) in Colombia, based on ecological niche modeling. *J Trop Med* 2016; 2016: 1439090.
52. Francischetti IM, Ribeiro JM, Champagne D, Andersen J. Purification, cloning, expression, and mechanism of action of a novel platelet aggregation inhibitor from the salivary gland of the blood-sucking bug, *Rhodnius prolixus*. *J Biol Chem* 2000; 274: 12639–50.
53. van de Locht A, Lamba D, Bauer M, Huber R, Friedrich T, Kröger B, Hojken W, Bode W. Two heads are better than one: crystal structure of the insect derived double domain Kazal inhibitor rhodniin in complex with thrombin. *EMBO J* 1995; 14: 5149–57.
54. Paim RM, Araújo RN, Soares AC, Lemos LC, Tanaka AS, Gontijo NF, Lehane MJ, Pereira MH. Influence of the intestinal anticoagulant in the feeding performance of triatomine bugs (Hemiptera; Reduviidae). *Int J Parasitol* 2011; 41: 765–73.
55. Isawa H, Yuda M, Yoneda K, Chinzei Y. The insect salivary protein, prolixin-S, inhibits factor IXa generation and Xase complex formation in the blood coagulation pathway. *J Biol Chem* 2000; 275: 6636–41.
56. Mizurini DM, Francischetti IM, Andersen JF, Monteiro RQ. Nitrophorin 2, a factor IX(a)-directed anticoagulant, inhibits arterial thrombosis without impairing haemostasis. *Thromb Haemost* 2010; 104: 1116–23.
57. Weichsel A, Andersen JF, Champagne DE, Walker FA, Montfort WR. Crystal structures of a nitric oxide transport protein from a blood-sucking insect. *Nat Struct Biol* 1998; 4: 304–9.
58. Maes EM, Roberts SA, Weichsel A, Montfort WR. Ultrahigh resolution structures of nitrophorin 4: heme distortion in ferrous CO and NO complexes. *Biochemistry* 2005; 44: 12690–9.
59. Knipp M, Zhang H, Berry RE, Walker FA. Overexpression in *Escherichia coli* and functional reconstitution of the liposome binding ferriheme protein nitrophorin 7 from the bloodsucking bug *Rhodnius prolixus*. *Protein Expr Purif* 2007; 54: 183–91.
60. Knipp M, Yang F, Berry RE, Zhang H, Shokhirev MN, Walker, FA. Spectroscopic and functional characterization of nitrophorin 7 from the blood-feeding insect *Rhodnius prolixus* reveals an important role of its isoform-specific N-terminus for proper protein function. *Biochemistry* 2007; 46: 13254–68.
61. Shelnutz JA, Song XZ, Ma JG, Jia SL, Jentzen W, Medforth CJ. Nonplanar porphyrins and their significance in proteins. *Chem Soc Rev* 1998; 27: 31–41.
62. Roberts SA, Weichsel A, Qiu Y, Shelnutz JA, Walker FA, Montfort WR. Ligand-induced heme ruffling and bent no geometry in ultra-high-resolution structures of nitrophorin 4. *Biochemistry* 2001; 40: 11327–37.
63. Kleingardner JG, Bren KL. Biological significance and applications of heme c proteins and peptides. *Acc Chem Res* 2015; 48: 1845–52.
64. Andersen JF, Gudderra NP, Francischetti IM, Valenzuela JG, Ribeiro JM. Recognition of anionic phospholipid membranes by an antihemostatic protein from a blood-feeding insect. *Biochemistry* 2004; 43: 6987–94.
65. Ding XD, Weichsel A, Andersen JF, Shokhireva TK, Balfour C, Pierik AJ, Averill BA, Montfort WR, Walker FA. Nitric oxide binding to the ferri- and ferroheme states of nitrophorin 1, a reversible NO-binding heme protein from the saliva of the blood-sucking insect, *Rhodnius prolixus*. *J Am Chem Soc* 1999; 121: 128–38.
66. Berry RE, Shokhirev MN, Ho AY, Yang F, Shokhireva TK, Zhang H, Weichsel A, Montfort WR, Walker FA. Effect of mutation of carboxyl side-chain amino acids near the heme on the midpoint potentials and ligand binding constants of nitrophorin 2 and its NO, histamine, and imidazole complexes. *J Am Chem Soc* 2009; 131: 2313–27.
67. Varadarajan R, Zewert TE, Gray HB, Boxer SG. Effects of buried ionizable amino acids on the reduction potential of recombinant myoglobin. *Science* 1989; 243: 69–72.
68. Nienhaus K, Maes EM, Weichsel A, Montfort WR, Nienhaus GU. Structural dynamics controls nitric oxide affinity in nitrophorin 4. *J Biol Chem* 2004; 279: 39401–7.
69. Hoshino M, Maeda M, Konishi R, Seki H, Ford PC. Studies on the reaction mechanism for reductive nitrosylation of ferrihemoproteins in buffer solutions. *J Am Chem Soc* 1996; 118: 5702–7.
70. Andersen JF, Weichsel A, Balfour CA, Champagne DE, Montfort WR. The crystal structure of nitrophorin 4 at 1.5 Å resolution: transport of nitric oxide by a lipocalin-based heme protein. *Structure* 1998; 6: 1315–27.
71. Maes EM, Weichsel A, Andersen JF, Shepley D, Montfort WR. Role of binding site loops in controlling nitric oxide release: structure and kinetics of mutant forms of nitrophorin 4. *Biochemistry* 2004; 43: 6679–90.
72. Eich RF, Li T, Lemon DD, Doherty DH, Curry SR, Aitken JF, Mathews AJ, Johnson KA, Smith RD, Phillips GN Jr, Olson JS. Mechanism of NO-induced oxidation of myoglobin and hemoglobin. *Biochemistry* 1996; 35: 6976–83.
73. Thorsteinsson MV, Bevan DR, Potts M, Dou Y, Eich RF, Hargrove MS, Gibson QH, Olson JS. A cyanobacterial hemoglobin with

- unusual ligand binding kinetics and stability properties. *Biochemistry* 1999; 38: 2117–26.
74. Foley EW. Physiologically relevant reaction of myoglobin and hemoglobin with NO. Houston: Rice University, 2006.
  75. Andersen JF, Champagne DE, Weichsel A, Ribeiro JM, Balfour CA, Dress V, Montfort WR. Nitric oxide binding and crystallization of recombinant nitrophorin I, a nitric oxide transport protein from the blood-sucking bug *Rhodnius prolixus*. *Biochemistry* 1997; 36: 4423–8.
  76. Lim MD, Lorkovic IM, Ford PC. NO and NO<sub>x</sub> interactions with group 8 metalloporphyrins. *J Inorg Biochem* 2005; 99: 151–65.
  77. Stamler JS, Lamas S, Fang FC. Nitrosylation. the prototypic redox-based signaling mechanism. *Cell* 2001; 106: 675–83.
  78. Swails JM, Meng Y, Walker FA, Marti MA, Estrin DA, Roitberg AE. pH-dependent mechanism of nitric oxide release in nitrophorins 2 and 4. *J Phys Chem B* 2009; 113: 1192–201.
  79. Menyhárd DK, Keserü GM. Protonation state of Asp30 exerts crucial influence over surface loop rearrangements responsible for NO release in nitrophorin 4. *FEBS Lett* 2005; 579: 5392–8.
  80. Schmidt HH, Walter U. NO at work. *Cell* 1994; 78: 919–25.
  81. Pacher P, Beckman JS, Liaudet L. Nitric oxide and peroxynitrite in health and disease. *Physiol Rev* 2007; 87: 315–424.
  82. Mannaioni PF, Bello MG, Di Bello MG, Schunack W, Masini E. Histamine up-regulates the generation of nitric oxide, and nitric oxide down-regulates the release of histamine in cardiovascular preparations. *Inflamm Res* 1997; 46: S97–8.
  83. Traverso L, Lavore A, Sierra I, Palacio V, Martinez-Barnetteche J, Latorre-Estivalis JM, Mougabure-Cueto G, Francini F, Lorenzo MG, Rodríguez MH, Ons S, Rivera-Pomar RV. Comparative and functional triatomine genomics reveals reductions and expansions in insecticide resistance-related gene families. *PLoS Negl Trop Dis*. 2017; 11: e0005313.
  84. Reinhardt K, Siva-Jothy MT. Biology of the bed bugs (Cimicidae). *Annu Rev Entomol* 2007; 52: 351–74.
  85. Delaunay P, Blanc V, Del Giudice P, Levy-Bencheton A, Chosidow O, Marty P, Brouqui P. Bedbugs and infectious diseases. *Clin Infect Dis* 2011; 52: 200–10.
  86. Boase C. Bedbugs back from the brink. *Pestic Outlook* 2001; 12: 159–62.
  87. Paul J, Bates J. Is infestation with the common bedbug increasing? *BMJ* 2000; 320: 1141.
  88. Lai O, Ho D, Glick S, Jagdeo J. Bed bugs and possible transmission of human pathogens: a systematic review. *Arch Dermatol Res* 2016; 308: 531–8.
  89. Weichsel A, Andersen JF, Roberts SA, Montfort WR. Nitric oxide binding to nitrophorin 4 induces complete distal pocket burial. *Nat Struct Biol* 2000; 7: 551–4.
  90. Åkerström B, Flower DR, Salier JP. Lipocalins: unity in diversity. *Biochim Biophys Acta* 2000; 18: 1–8.
  91. Diarra-Mehrpour M, Bourguignon J, Sesboue R, Mattei MG, Passage E, Salier JP, Martin JP. Human. Plasma inter- $\alpha$ -trypsin inhibitor is encoded by four genes on three chromosomes. *Eur J Biochem* 1989; 179: 147–54.
  92. Kaumeyer JF, Polazzi JO, Kotick MP. The mRNA for a proteinase inhibitor related to the HI-30 domain of inter- $\alpha$ -trypsin inhibitor also encodes  $\alpha_1$ -microglobulin (protein HC). *Nucleic Acids Res* 1986; 14: 7839–50.
  93. Lindqvist A, Bratt T, Altieri M, Kastern W, Åkerström B. Rat  $\alpha_1$ -microglobulin: co-expression in liver with the light chain of inter- $\alpha$ -trypsin inhibitor. *Biochim Biophys Acta* 1992; 1130: 63–7.
  94. Åkerström B, Lögdberg L. An intriguing member of the lipocalin protein family:  $\alpha_1$ -microglobulin. *Trends Biochem Sci* 1990; 15: 240–3.
  95. Ekström B, Berggård I. Human  $\alpha_1$ -microglobulin. Purification procedure, chemical and physicochemical properties. *J Biol Chem* 1977; 252: 8048–57.
  96. Åkerström B, Gram M. A1M, an extravascular tissue cleaning and housekeeping protein. *Free Radic Biol Med* 2014; 74: 274–82.
  97. Grubb A, Méndez E, Fernandez-Luna JL, López C, Mihaesco E, Vaerman JP. The molecular organization of the protein HC-IgA complex (HC-IgA). *J Biol Chem* 1986; 25: 14313–20.
  98. Allhorn M, Klapayta A, Åkerström B. Redox properties of the lipocalin  $\alpha_1$ -microglobulin: reduction of cytochrome c, hemoglobin, and free iron. *Free Radic Biol Med* 2005; 38: 557–67.
  99. Åkerström B, Maghzal GJ, Winterbourn CC, Kettle AJ. The lipocalin  $\alpha_1$ -microglobulin has radical scavenging activity. *J Biol Chem* 2007; 282: 31493–503.
  100. Rutardottir S, Nilsson EJ, Pallon J, Gram M, Åkerström B. The cysteine 34 residue of A1M/ $\alpha_1$ -microglobulin is essential for protection of irradiated cell cultures and reduction of carbonyl groups. *Free Radic Res* 2013; 47: 541–50.
  101. Allhorn M, Berggård T, Nordberg J, Olsson ML, Åkerström B. Processing of the lipocalin  $\alpha_1$ -microglobulin by hemoglobin induces heme-binding and heme-degradation properties. *Blood* 2002; 99: 1894–901.
  102. Allhorn M, Lundqvist K, Schmidtchen A, Åkerström B. Heme-scavenging role of  $\alpha_1$ -microglobulin in chronic ulcers. *J Investig Dermatol* 2003; 121: 640–6.
  103. Escribano J, Lopex-Otin C, Hjerpe A, Grubb A, Mendez E. Location and characterization of the three carbohydrate prosthetic groups of human protein HC. *FEBS Lett* 1990; 266: 167–70.
  104. Meining W, Skerra A. The crystal structure of human  $\alpha_1$ -microglobulin reveals a potential haem-binding site. *Biochem J* 2012; 445: 175–82.
  105. Skerra A. Lipocalins as a scaffold. *Biochim Biophys Acta* 2000; 18: 337–50.
  106. Berggård T, Cohen A, Persson P, Lindqvist A, Cedervall T, Silow M, Thøgersen IB, Jönsson JA, Enghild JJ, Åkerström B.  $\alpha_1$ -Microglobulin chromophores are located to three lysine residues semiburied in the lipocalin pocket and associated with a novel lipophilic compound. *Protein Sci* 1999; 8: 2611–20.
  107. Kwasek A, Osmark P, Allhorn M, Lindqvist A, Åkerström B, Wasylewski Z. Production of recombinant human  $\alpha_1$ -microglobulin and mutant forms involved in chromophore formation. *Protein Expr Purif* 2007; 53: 145–52.
  108. Rutardottir S, Karnaukhova E, Nantassenamat C, Songtawee N, Prachayasittikul V, Rajabi M, Rosenlöf LW, Alayash AI, Åkerström B. Structural and biochemical characterization of two heme binding sites on  $\alpha_1$ -microglobulin using site directed mutagenesis and molecular simulation. *Biochim Biophys Acta* 2016; 1864: 29–41.
  109. Calero M, Escribano J, Grubb A, Mendez E. Location of a novel type of interpolypeptide chain linkage in the human protein HC-IgA complex (HC-IgA) and identification of a heterogeneous chromophore associated with the complex. *J Biol Chem* 1994; 269: 384–9.
  110. Zhang Y, Gao Z, Guo Z, Zhang H, Zhang Z, Luo M, Hou H, Huang A, Dong Y, Wang D. The crystal structure of human protein  $\alpha_1$ M reveals a chromophore-binding site and two putative protein-protein interfaces. *Biochem Biophys Res Commun* 2013; 439: 346–50.

111. Theologis A, Ecker JR, Palm CJ, Federspiel NA, Kaul S, White O, Alonso J, Altafi H, Araujo R, Bowman CL, Brooks SY, Buehler E, Chan A, Chao Q, Chen H, Cheuk RF, Chin CW, Chung MK, Conn L, Conway AB, Conway AR, Creasy TH, Dewar K, Dunn P, Etgu P, Feldblyum TV, Feng J, Fong B, Fujii CY, Gill JE, Goldsmith AD, Haas B, Hansen NF, Hughes B, Huizar L, Hunter JL, Jenkins J, Johnson-Hopson C, Khan S, Khaykin E, Kim CJ, Koo HL, Kremenskaia I, Kurtz DB, Kwan A, Lam B, Langin-Hooper S, Lee A, Lee JM, Lenz CA, Li JH, Li Y, Lin X, Liu SX, Liu ZA, Luros JS, Maiti R, Marziali A, Militscher J, Miranda M, Nguyen M, Nierman WC, Osborne BI, Pai G, Peterson J, Pham PK, Rizzo M, Rooney T, Rowley D, Sakano H, Salzberg SL, Schwartz JR, Shinn P, Southwick AM, Sun H, Tallon LJ, Tambunga G, Toriumi MJ, Town CD, Utterback T, Van Aken S, Vaysberg M, Vysotskaia VS, Walker M, Wu D, Yu G, Fraser CM, Venter JC, Davis RW. Sequence and analysis of chromosome 1 of the plant *Arabidopsis thaliana*. *Nature* 2000; 408: 816–20.
112. Hargrove MS, Olson JS. The stability of holomyoglobin is determined by heme affinity. *Biochemistry* 1996; 35: 11310–8.
113. Roussigne M, Kossida S, Lavigne AC, Clouaire T, Ecochard V, Glories A, Amalric F, Girard JP. The THAP domain: a novel protein motif with similarity to the DNA-binding domain of P element transposase. *Trends Biochem Sci* 2003; 28: 66–9.
114. Clouaire T, Roussigne M, Ecochard V, Mathe C, Amalric F, Girard JP. The THAP domain of THAP1 is a large C2CH module with zinc-dependent sequence-specific DNA-binding activity. *Proc Natl Acad Sci USA* 2005; 102: 6907–12.
115. Dangl J. Innate immunity. Plants just say NO to pathogens. *Nature* 1998; 394: 525–7.
116. Delledonne M, Xia Y, Dixon RA, Lamb C. Nitric oxide functions as a signal in plant disease resistance. *Nature* 1998; 394: 585–8.
117. Wendehenne D, Durner J, Klessig DF. Nitric oxide: a new player in plant signalling and defence responses. *Curr Opin Plant Biol* 2004; 7: 449–55.
118. Onoda A, Fukumoto K, Arlt M, Bocola M, Schwaneberg U, Hayashi T. A rhodium complex linked  $\beta$ -barrel protein as a hybrid biocatalyst for phenylacetylene polymerization. *Chem Commun* 2012; 48: 9756–8.
119. Onoda A, Kihara Y, Fukumoto K, Yohei S, Hayashi T. Photoinduced hydrogen evolution catalyzed by a synthetic diiron dithiolate complex embedded within a protein matrix. *ACS Catal* 2014; 4: 2645–8.
120. Himiyama T, Sauer DF, Onoda A, Spaniol TP, Okuda J, Hayashi T. Construction of a hybrid biocatalyst containing a covalently-linked terpyridine metal complex within a cavity of aponitrobindin. *J Inorg Biochem* 2016; 158: 55–61.
121. Fukumoto K, Onoda A, Mizohata E, Bocola M, Inoue T, Schwaneberg U, Hayashi T. Rhodium-complex-linked hybrid biocatalyst: stereo-controlled phenylacetylene polymerization within an engineered protein cavity. *ChemCatChem* 2014; 6: 1229–35.
122. Winter A, Newkome GR, Schubert US. Catalytic applications of terpyridines and their transition metal complexes. *ChemCatChem* 2011; 3: 1384–406.
123. Zhang C, Srivastava P, Ellis-Guardiola K, Lewis JC. Manganese terpyridine artificial metalloenzymes for benzylic oxygenation and olefin epoxidation. *Tetrahedron* 2014; 70: 4245–9.